

RECENT PLANETARY TOPOGRAPHIC MAPPING AT THE USGS, FLAGSTAFF: MOON, MARS, VENUS, AND BEYOND

Randolph L. Kirk, Elpitha Howington Kraus, and Mark Rosiek

U.S. Geological Survey, Astrogeology Team

rkirk@usgs.gov

Working Group IV/5

KEY WORDS: Extraterrestrial Mapping, Softcopy Photogrammetry, Moon, Mars, Venus

ABSTRACT

We are currently using stereophotogrammetric techniques to compile digital topographic models of parts of the Moon, Mars, Venus, and the asteroid Eros in support of the NASA program of planetary exploration. This work requires the synergistic use of the USGS digital cartographic software system ISIS for data ingestion and calibration steps, along with the commercial software SOCET SET® for “photogrammetric” steps such as adjustment of control and topographic model extraction and editing. Novel procedures must frequently be developed to deal with problems of planetary datasets such as the need to use large numbers of small images, nonuniform image coverage, poor image overlap, and lack of true ground control. Some sensors, such as the Magellan Synthetic Aperture Radar, also require the development of specialized sensor model software.

An important theme of our work is the complementarity between photogrammetric techniques and the laser altimeter systems coming into increasing use on planetary spacecraft. Stereoanalysis of Clementine images of the Moon has been used to fill in major gaps in the altimeter dataset at high latitudes, but the stereo data must be tied to the altimetry where the datasets overlap. For Mars and Eros, our stereomapping provides spatial sampling of topography finer than that achieved by altimetry, but use of the altimetry data for vertical control can significantly improve the absolute accuracy of photogrammetric topographic models.

This work was completed using a photogrammetric software system, SOCET SET® from LH Systems. Any use of trade, product, or firm names is for descriptive purposes only and does not imply endorsement by the U.S. Government.

1 INTRODUCTION

In this paper we report on recent planetary stereotopographic mapping conducted by the Planetary Geomatics Group of the Astrogeology Team, U.S. Geological Survey, Flagstaff, Arizona. The Astrogeology Team (formerly Branch of Astrogeology) has a long history of research and production in planetary photogrammetry (Wu and Doyle, 1990), beginning with lunar mapping in support of the Apollo program and, in the early 1970s, the production of the first topographic maps of Mars (Wu, 1975). Despite the routine use of digital imaging in planetary missions, the photogrammetric aspects of this work were carried out with the analytic-plotter technology of the day by using film output from the digital data. Topographic mapping of Mars at a variety of scales with Viking Orbiter images continued throughout the 1970s and 1980s, culminating in the release of a global digital topographic model of the planet (USGS, 1991; Batson and Eliason, 1991) that was generated by digitizing and interpolating hardcopy contour data. By the mid-1990s, the OMI AS-11 plotters that had been used for this work were reaching the end of their mechanical and electronic lifespans. At the same time, the all-digital or “softcopy” photogrammetric systems that were becoming available promised greatly improved mapping productivity and (because they were based on off-the-shelf computer hardware) reduced costs. These softcopy systems were particularly attractive for planetary work, given that the imagery of interest was already digital so we did not face the obstacle of having to scan large volumes of film. We therefore sought a commercial off-the-shelf digital photogrammetric workstation that—suitably augmented with our own software and procedures—would be capable of planetary stereomapping. In December 1996 we took delivery of a Leica/Helava (now LH Systems) DPW 790 workstation running their SOCET SET® software and began the task of adapting it to our needs. The initial hardware configuration, used for most of the lunar and Venus work reported here, consisted of a Silicon Graphics Indy XGE R5000 computer graphics workstation with 126 Mbytes of memory and 476 Mbytes of swap space. We are currently transitioning to a Sun Ultra 10 Model 440 with 1 Gbyte of memory and 2 Gbytes of swap space, resulting in a nearly fivefold improvement in processing speed.

The capabilities of a typical softcopy photogrammetric system (stereo image display with 3D input device for interaction; manual and automatic point measurement; aerotriangulation; manual and automatic extraction of digital

topographic models or DTMs, etc.) are undoubtedly well known to the present readership. The unique requirements of planetary stereomage data may be less well known and form the focus of this article. Briefly, the challenges we have encountered can be divided into the following three categories.

- *Multiplicity of datasets.* The imaging systems flown on planetary spacecraft missions are almost always developed uniquely for a single mission, resulting in a host of datasets that differ not only in their geometric properties but also in the methods required for radiometric/geometric calibration and other preprocessing, as well as the formats in which the image data and metadata (including orientation parameters) are stored.
- *Novel sensors.* Many planetary missions have utilized framing camera systems that can be modeled with the same software used for “conventional” aerial photography, but important stereo datasets have been obtained from other types of sensors (e.g., Magellan synthetic aperture radar, Mars Orbiter Camera pushbroom scanner) and others are planned for the future (Mars Express HRSC multiline stereo scanner).
- *Unusual geometric and coverage properties.* Operational requirements of planetary missions often result in image coverage with widely varying resolutions and viewing geometries, gaps in coverage, and poor image overlap. Planetary cameras are often designed with extremely narrow fields of view, necessitating oblique imaging to obtain stereo convergence, and the individual images from digital framing cameras are typically very small (200–1000 pixels on a side), requiring the use of many images to cover an area of interest. The lack of true ground control (apart from a few landing sites on the Moon and Mars) also falls in this category.

The first and second types of challenges must be met by development of software for image preprocessing/ingestion and for defining new sensor models, respectively. Dealing with the geometric properties and nonideal coverage of planetary data primarily requires innovative approaches to developing new procedures for each dataset (though in practice new software is often needed to implement these procedures). A crucial part of our approach to planetary topomapping is the synergistic use of the SOCET SET commercial photogrammetric software with the USGS software system ISIS (Integrated Software for Imagers and Spectrometers) (Eliason, 1997; Gaddis, et al. 1997; Torson and Becker, 1997). ISIS combines basic capabilities of image processing, analysis and display of 2- and 3- dimensional (multispectral and hyperspectral) data with specialized planetary cartographic functionality. The system already contains a large number of specialized programs to carry out mission- and sensor-specific processing steps such as ingesting and cataloguing images and performing radiometric and geometric calibration for data from numerous missions including Mariner, Viking, Voyager, Galileo, Clementine, Mars Pathfinder, and Mars Global Surveyor. Because the software is developed in-house, new modules can be added rapidly as needed to address additional missions and datasets. In the following section, we discuss in some detail the interface that we have created between the ISIS and SOCET SET systems, and how data for planetary framing cameras in particular is transferred from one to the other. Subsequent sections discuss several of our current mapping projects, involving the Moon, Mars, Venus, and the asteroid Eros. To varying degrees our experiences with these projects emphasize the need for new procedures and new software such as sensor models. Readers interested in an additional case study are directed to papers by Kirk et al. (1999c) and Gaddis et al. (1999) that deal with the processing of panoramic stereomage from the Mars Pathfinder mission, which was the first project undertaken with the combination of ISIS and SOCET SET software.

2 SOFTWARE AND PROCEDURES FOR FRAMING CAMERAS: GENERAL CONSIDERATIONS

Augmenting LH Systems’ SOCET SET digital photogrammetric system (Miller and Walker, 1993; 1995) for photogrammetric mapping of the planets is fairly straightforward when imaging instruments employed by planetary exploration missions behave as framing cameras, such as the CCD array used in Clementine or the Viking Orbiter vidicon cameras. The necessary adaptations are carried out in two areas. First and fundamentally, geodetic information of the planets and satellites, mapping projection parameters, and camera definitions must be supplied to SOCET SET. Second, an interface between ISIS and SOCET SET is needed so that the strengths of each system can be easily utilized. The interface between the two systems consists of routines and procedures to import/export image data and associated geometric information; auxiliary data files needed for triangulation; and advanced data products such as DTMs and orthophoto mosaics. Further information on ISIS can be found at the following web site: [http://wwwflag.wr.usgs.gov/isis-bin/isis.cgi](http://www.flag.wr.usgs.gov/isis-bin/isis.cgi).

SOCET SET is designed with an internal database directory that stores a suite of static data used to control a variety of SOCET SET functions. These are text files; so adapting SOCET SET to map spherical or near-spherical bodies involves appending planetary reference datums (as radius and eccentricity squared) to the files defining standard Earth reference datums. This is a one-time effort with each new release of SOCET SET and allows the operator selection of a planet figure, by planet or satellite name, at the time a mapping project is being defined. In addition to planetary geodetic information, definitions of grid coordinate systems specific to a planet must be created for subsequent use in SOCET SET. The definitions needed for planetary mapping are appended to a file of existing grid coordinate systems for Earth and consist of a “grid name” (used for operator selection during project creation), the planet radius and eccentricity

squared, and the map projection along with its associated parameters. Typical planetary mapping products are produced in Mercator, Transverse Mercator, Lambert Conformal, Polar Stereographic or Sinusoidal map projections. The last data file required by SOCET SET contains camera specifications (i.e., focal length, fiducial coordinates, lens distortion coefficients, etc.). Because of the variety of aerial framing cameras, SOCET SET provides a camera editor where the operator may enter the camera specifications via a GUI (Graphical User Interface) and then save the information to a file in the internal database.

Preparing a planetary image for import to SOCET SET requires several steps in ISIS. First, the native format of the image and support data must be converted using ISIS routines to an ISIS formatted image. Each ISIS image consists of a label area where all the parameters that describe the image are stored as keywords followed by their respective values. Included in the ISIS package are a variety of image processing routines that have been developed for general image enhancement, for mission specific radiometric calibration of imagery, and for the correction of mission specific distortions that may exist, such as camera geometry distortions. Although quantitative radiometric calibration is obviously not a requirement for stereomapping, the radiometric calibration process also serves to remove both broad shading variations and high-frequency detail due to irregularities in the camera detector, both of which can affect the performance of automatic stereomatching. Geometric calibration is commonly performed in ISIS for vidicon sensors (as flown on the Mariner, Voyager, and Viking spacecraft), which are subject to complex, scene-dependent distortions. Correction of these distortions is based on the array of reseau marks placed at known locations on the focal plane of the detector. Automatic matching of reseau templates to the images is used to determine the reseau locations in the distorted image, after which the image is resampled so as to restore the reseaux to their ideal, undistorted positions. The optical distortion of the lens can also be corrected in the resampling step, but if the reseau correction is not needed (i.e., for a CCD camera as flown on Clementine) the lens distortion may be handled by including a distortion polynomial in the SOCET SET camera definition. Once an image has been ingested and calibrated in ISIS, it is ready for import into SOCET SET.

When importing an image in SOCET SET, known camera position and orientation can be supplied. Camera positions and orientations exist on the labels of ISIS images but in coordinate systems not recognized by SOCET SET. ISIS stores the camera position as a vector in Earth Mean Equatorial (EME) coordinates. EME is an inertial coordinate system (or reference frame) in which the equations of motion for the solar system may be integrated. EME is specified by the orientation of the Earth's mean equator and equinox at a particular epoch – typically the J2000 epoch. The J2000 epoch is Greenwich noon on January 1, 2000 Barycentric Dynamical Time. (Barycentric Dynamical Time is believed to be in agreement with the time that would be kept by an atomic clock located at the solar system barycenter, i.e., the time at the center of mass around which bodies in the solar system rotate.) For use in SOCET SET, the ISIS camera positions are converted to planetographic coordinates (specifically, longitude and latitude relative to the center of a planet, and height above the planet datum). Attention must be given to the resulting longitude coordinate of the camera position. For many planets, the direction of positive longitude is defined to be positive-west, whereas SOCET SET expects longitudes to be entered as positive-east, such as is the definition on Earth. When positive longitudinal direction conflicts with that of Earth, the longitude signs must be changed upon import to and export from SOCET SET. As for camera orientation angles, these are stored in ISIS as right-ascension, declination and twist (RA, Dec, Twist) angles, which define the transform between EME coordinates and camera coordinates. SOCET SET expects camera orientation angles that define the transformation from ground space (planet surface) to image space, so the ISIS camera orientation angles are converted to the photogrammetrically familiar omega-phi-kappa rotation system.

Once the coordinate system conversions have taken place, the ISIS image is stripped of its labels and imported as a raw-binary file into SOCET SET—along with the known camera position and orientation coordinates. During image import, SOCET SET allows the operator the option to enable atmospheric refraction corrections. For planetary mapping, the operator chooses not to apply atmospheric correction because the default atmospheric correction in SOCET SET is Earth specific; in addition, most planets have little or no atmosphere. (For planets that have an appreciable atmosphere, such as Venus, the planet's specific atmospheric corrections can be incorporated in a custom sensor model. LH Systems offers a Developer's Toolkit that enables their customers to write and incorporate custom sensor models into SOCET SET, as discussed below.)

Other datasets that can be imported/exported between SOCET SET and ISIS consist of image point coordinate and ground point coordinate files used in bundle-block adjustments. (Image triangulation routines in ISIS are targeted for the production of planetary image mosaics—a two dimensional product wherein the overlap requirement between adjacent images can be minimal.) ISIS stores all the image point measurements for a mapping project in a single "match point" file. To identify which image a given image point measurement is on, the match point file lists the "image number", not the filename, of the image. (The image number is stored in the label area of an ISIS image and is unique to each image.) Conversely, SOCET SET is designed to store image point measurements in a separate file for each image in a project, and the actual filenames of the SOCET SET images are used to identify which image a point

measurement is on. Importing ISIS match point files into SOCET SET requires mapping the ISIS image numbers to SOCET SET image filenames and creating multiple image point files.

Ground point coordinates for an ISIS project are also stored in a single file, which is the same approach SOCET SET takes. Importing an ISIS ground point file into SOCET SET involves reformatting the ground point information (with attention given to the direction of positive longitude as is the case of camera positions), and adding parameters expected by SOCET SET's MST (Multi Sensor Triangulation), such as weights associated with each point and various flags that indicate whether a point is a control point, tie point or check point. Tie points measured in ISIS for the purpose of making image mosaics can be used as horizontal control in SOCET SET. Typically, tie points measured in ISIS exist between two images only, so to strengthen exterior orientation results in SOCET SET, these points can be propagated to other overlapping images by automatic point measurement techniques in SOCET SET. When laser altimetry data exists for a planet, it can be combined with ISIS tiepoints through interpolation techniques to provide vertical control for SOCET SET. An altimetry point also can be directly used as full 3D control, if the position of the altimetry point can be visually (and reliably) identified on an image, e.g., if it occupies the bottom of an impact crater (Duxbury et al., 1999).

Modifications were made to the parameter files used by SOCET SET correlation software in Automatic Point Measurement (APM), Interactive Point Measurement (IPM) and Automatic Terrain Extraction (ATE) modules. Since planetary framing camera images are small in size, not all the reduced resolution sets that are normally expected by the correlation software are available. In addition, the search window size needs to be set at an appropriate size for smaller images.

3 EARTH'S MOON

Topographic mapping of the lunar poles has been a major focus of our efforts for the last two years. The Clementine data consist of conventional (albeit relatively narrow-angle) framing-camera images and do not pose any conceptual novelties. Considerable effort was necessary, however, to develop a successful approach to constructing a photogrammetric control network that covers the pole and connects to altimetric elevation data available at lower latitudes. We believe that the effort to derive such a control network is warranted by the strong scientific interest aroused by the possible discovery of ice at the lunar poles (Nozette et al., 1996; Feldman et al., 1998; but see also Simpson and Tyler, 1999). Previous attempts to derive topographic models of the south pole of the Moon from Clementine imagery that have relied on unadjusted orientation data (Wählisch et al., 1999) or sequential adjustment of overlapping DTM segments (Cook et al., 1999; 2000b) rather than least-squares adjustment of a control network have produced elevations for the pole that differ by several kilometers from one another and from non-photogrammetrically derived elevations (Margot et al., 1999). A rigorously derived photogrammetric control network of the lunar poles may not resolve this discrepancy but should clearly indicate the level of confidence to be attached to the resulting topography.

3.1 Clementine Mission and Data

The Clementine mission was conceived in 1992 by the National Aeronautics and Space Administration (NASA), U.S. Department of Defense, and industry to test new lightweight spacecraft technology. The goal was to acquire data that would assist in determining the mineral content of the Moon and a near-Earth asteroid. In 1994, the Clementine spacecraft acquired digital images of the Moon at visible and near infrared wavelengths (Nozette et al., 1994). On board there were four camera systems and a laser altimeter. During the first month, periapsis was at 30°S and the highest resolution images were obtained in the southern hemisphere (Cook et al., 1996). Over the northern polar area a series of oblique and nadir images was obtained with the ultraviolet-visible (UVVIS) camera on each orbit. During the second month, periapsis was at 30°N and image acquisition was reversed, with high-resolution images in the north and oblique and nadir images in the south.

The laser altimeter (LIDAR) system was sighted through the high-resolution (HIRES) camera optics. The estimated error in an individual range measurement is between 100 and 130 m. Altimeter data were collected between 79°S and 81°N. Over some smooth mare surfaces, an along-track spacing of 20 km was achieved but where the instrument lost lock over rough terrain the spacing degraded to 100 km. The across-track spacing was based on the orbital track and is approximately 60 km at the equator, decreasing toward the poles. A global topographic model was derived based on spherical harmonic expansion (Zuber et al., 1994; Smith et al., 1997); the gaps at the poles where data were not collected are filled in this model by interpolation.

The combination of cameras and filters on Clementine resulted in nearly 1 million images in the 11 visible and near-infrared spectral bands, 620,000 high-resolution images and 320,000 long-wave infrared images. These datasets include both global, nadir-looking multispectral imagery of interest for geologic and compositional studies of the surface, and

stereo coverage suitable for topographic mapping of a large fraction of the Moon, including both poles. Mosaicking of the global, multispectral data at the USGS required the development of software and databases that contribute significantly toward the topographic mapping described here. The first product generated was a global mosaic of the UVVIS 750 nm images. Match points were picked to tie the images together, and the camera pointing angles were adjusted to align the images. This adjustment used a spherical surface, and the elevation for tie points was held to a constant value, 1737.4 km. This produced a seamless image mosaic with latitude and longitude information but no information on the elevation (Eliason, 1997; Isbell et al., 1997). Mosaics of the other UVVIS bands were subsequently tied to the 750 nm base, and NIR mosaics are currently in production (Eliason et al., 1999; Isbell et al., 1999). The database of Clementine images generated as an aid to producing these mosaics contains information about each image including camera, filter, gain state, time of acquisition, orbit, ground sample distance, latitude and longitude of center point, and the emission angle (an angle between a local surface normal and a vector to the camera system). This database was essential in choosing images for stereomapping.

The UVVIS camera image size was 384x288 pixels with five spectral bands and one broad band. The 750 nm band oblique/nadir pairs were the primary image source for this study. On an oblique image the ground sample distance (GSD) ranged from 300 to 400 meters. The GSD for the nadir images acquired at the end of an orbit were slightly larger and ranged from 325 to 450 meters. Using the formula for stereo height accuracy (Cook et al. 1996) an estimate of height accuracy is 180 m.

3.2 Triangulation and DTM Extraction

The size and unique characteristics of the Clementine polar stereo dataset required considerable experimentation to arrive at a satisfactory procedure for generating the needed geodetic control. For the south polar region, the initial dataset consisted of 6,406 images (nadir images from month one and both oblique and nadir from month two) and 29,386 match points used in producing the mosaic which were adopted as control points. The image list was reduced to 3,635 images by eliminating the images that were not used in making the global mosaic. All the match points on the selected images were used, and there was no check to see if the control points still fell on two images within the selected set of images. As images were eliminated, some match points ended up on only one image. This dataset was further reduced as explained below.

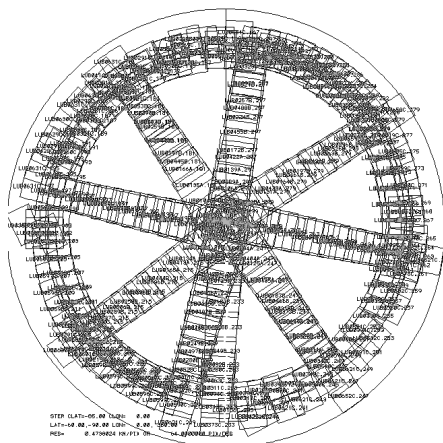


Figure 1. Control web for lunar south pole

overlaid. The majority (3/4) of control points were on two images, the remaining 1/4 of the points were only on one image. In order to remove the mismatch between stereo models the control points would have to be propagated to the other images that overlay the points.

SOCET SET has software to automatically transfer points between images but in tests mismatches occurred and some points failed to transfer. The reasons for these errors were easier to understand than to remedy. Instead of taking on the enormous job of transferring 29,000 points a decision was made to thin the control points, transfer the thinned points to the other images, add tie points if necessary, and eliminate points that were measured on only one image. The images were thinned to 978 oblique/nadir images from month two. The control points were thinned to between 6 and 2 per image, 1265 in total. The point transfer software was used to add 1200 more tie points. This software will divide an image into a 3 by 3 array of cells and add a tiepoint to any cell that does not already contain one.

The full dataset was too large for the analytical triangulation software. The images were therefore broken up into blocks and adjusted in a systematic way. The initial block formed a web over the entire area (Figure 1). The remaining blocks were wedge-shaped and filled the gaps between the legs of the webs. For the initial block, the camera angles for all images were adjusted. For the remaining blocks, the camera angles of the images common to the initial block were held fixed and the camera angles of the interior images were allowed to change.

First Run: The results of the analytical triangulation for all the blocks showed a root mean square (RMS) of 0.3 pixel with a maximum residual of 2.3 pixels (Rosiek et al., 1999a). When DTMs were collected from stereo models the overlap areas had disagreement in the elevation values of 2–3 km. The problem was most likely that the stereo models were displaced relative to each other because of the control points. Although the control points were used and adjusted during the process of forming the global mosaic, they were not transferred to other images they

Second Run: Computer memory was adequate for analytical triangulation of 978 images and ~2400 match points, which required ~3.5 hours on the Silicon Graphics workstation (Rosiek et al., 1999b). The process was to run the analytical triangulation, check the points with the largest residuals, and then rerun the analytical triangulation. After a few runs there were no points showing up with obvious blunders. Then all the match points were manually checked to ensure that each point was transferred to all images containing it, as the automatic transfer software did not always insure this.

After a stable solution was found for the analytical triangulation DTM collection could begin. The stereo models were based on the oblique and nadir images collected during the same orbit. Although it is possible for SOCET SET to be given a list of images and to automatically derive the DTM from the best pair of images, this software did not work with the Clementine images. The easiest solution was to set up each pair as a model and collect the DTM for that pair. To collect 1,764,996 DTM points from 616 stereo models in batch mode took 8 hours of computer time, after a few days spent manually setting up the DTM boundaries for each model. An advantage is that when the analytical triangulation was recomputed the DTMs could be recollected in batch mode. The DTMs collected from images in the same orbit were merged together. Quality control and editing for errors were done on these merged DTMs. The DTMs from each orbit were merged together into 8 sections and finally the sections were merged.

When the resulting DTM was compared with the altimetry data and the topography derived by Dr. Tony Cook (Cook et al., 2000b), systematic discrepancies were noted. Our DTM was higher at the outside edges (between 65°S and 75°S) than the altimetry data and the data from Cook but lower poleward of 80°S. Upon studying our triangulation results closely, we discovered that the tie points had not changed significantly in elevation but the control points had changed significantly and systematically in elevation despite being more tightly weighted. Since the camera angles were adjusted for the global mosaic and the tie point ground locations were determined from those camera angles, the difference on the weights of the control and tie points was not large enough and the adjustment stayed at the former adjustment for a spherical moon. To obtain a better solution for the analytical triangulation the weights on the control point elevation (Z) values would be lower and the camera angles would be reset to the values prior to the adjustment for the global mosaic.

Third run: The concept for the next analytical triangulation was to use two passes (Rosiek et al., 2000). The initial pass would be performed with artificially low Z sigmas of 20 m for the control points whose Z values were based on the Clementine altimetry data. The final pass would use realistic weights (Z sigma of 10,000 m) and allow the model to adjust. Using this type of weighting would align the results with the global mosaic and altimetry data. In addition, during the final pass the results of the initial run would provide better estimates for the tie points' ground locations.

The DTMs were recollected and merged. The 572 individual DTMs had an RMS error of 836 m and a standard deviation of 155 m where they overlapped along each orbit. The 50 DTMs that were merged between orbits had an RMS error of 391 m and a standard deviation of 351 m. The merged DTM was overlain with a Clementine south pole mosaic to check the alignment (Figure 2). Some errors can be seen in the concentric rings formed due to a bias in the elevation values. The contour lines align well with the craters, however, indicating that planimetric control is consistent with the base mosaic. During editing of the merged DTMs, a systematic bias was discovered: models closer to the poles were biased with higher elevation values than adjacent models farther from the pole. One plausible cause of this bias is the inadequate distribution of control points caused by the small (and in some cases nonexistent) overlap between stereomodels, leading to a control network geometry that is not strong enough for the standard process of least-squares adjustment of orientation parameters to remove the errors in the starting estimate of elevation. We are therefore developing a novel approach based on adjusting the elevations of overlapping DTM segments and then calculating orientations consistent with the adjustment to the DTM. It is also possible, however, that some of the elevation bias results from systematic errors in the spacecraft orbit information.

Fourth Run: To remove the systematic bias errors the DTMs will be adjusted with a least squares program that will offset each DTM in elevation so as to minimize the discrepancies both between overlapping DTM segments and between the DTM and the Clementine altimetry data. This program is derived from the existing ISIS program EQUALIZER, which is used to adjust the brightness and contrast of overlapping images before mosaicking. The elevation values from the merged DTM generated after this adjustment will be used as estimates for the match point elevation values in another analytical triangulation run. The match point sigmas will be set artificially low and the sigmas on the camera position and attitude will be set high so the position and attitude values will be adjusted. The sigmas for the match point position will then be set to a realistic value and the analytical triangulation will be run for a second pass. This process should both remove the bias between DTMs in each orbit and provide camera angles consistent with the corrected DTMs.

Data collection procedures will be slightly modified for collecting topography over the lunar north pole. The number of match points that are transferred from the ISIS files will increase. This will reduce the number of tie points that are

used. In order to tie the model together the higher resolution nadir images will need to be used in areas where the oblique/nadir images do not exist. Stereo coverage for both poles contains gaps, so in order to produce final digital terrain models with the same map boundaries as the Clementine mosaics, we will fill the gaps either with interpolated laser altimeter data or with data derived by photoclinometry. In areas of suitably uniform albedo imaged with oblique illumination, photoclinometry, or shape-from-shading (Kirk, 1987), can produce relative topographic models at the full resolution of the images used, but the method does not provide any information about absolute elevations. Any photoclinometric DTMs will therefore be merged with the stereo DTMs by adjusting their overall elevation with the least-squares procedure described above.

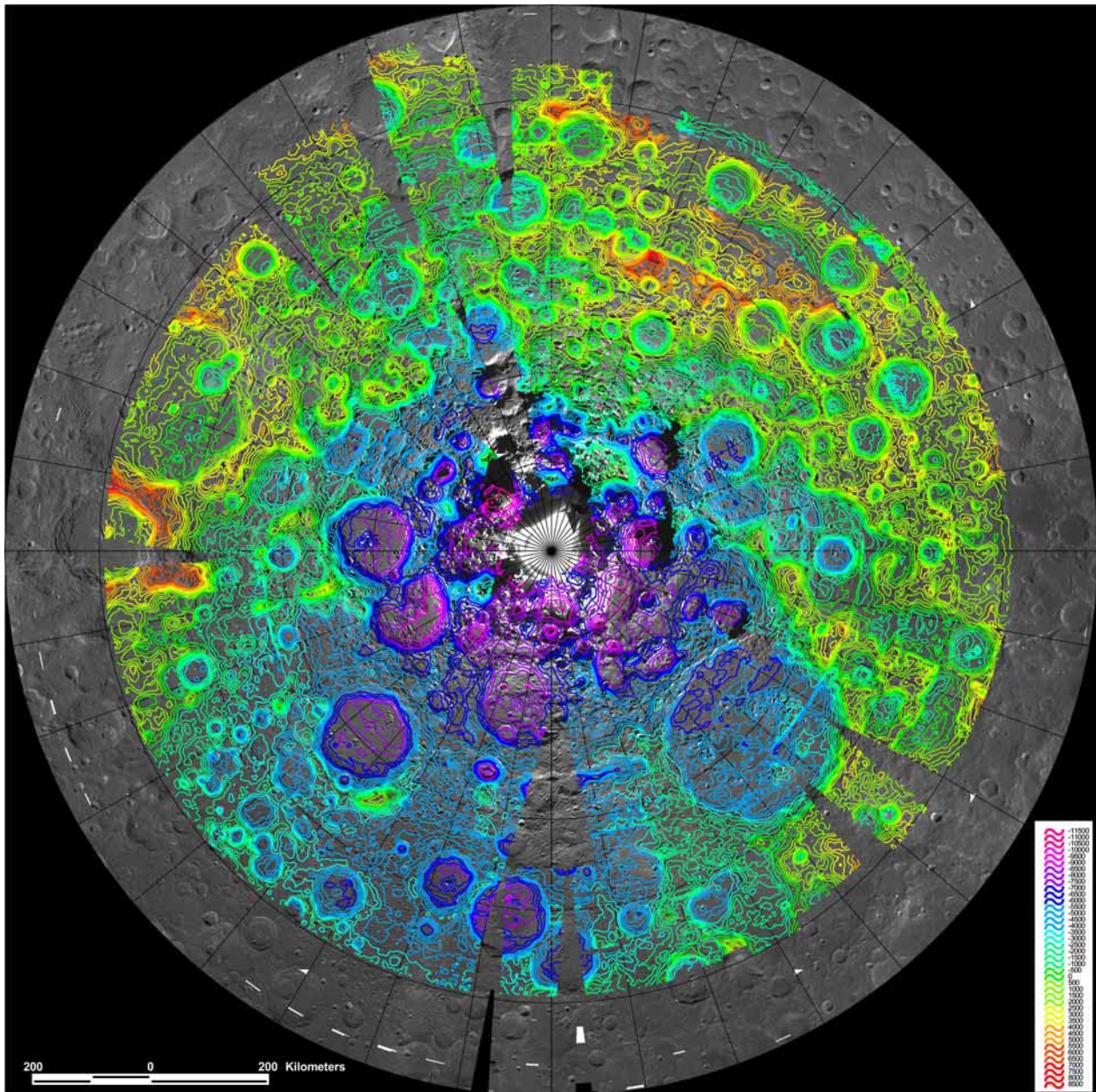


Figure 2. Contour lines for the lunar south pole derived from the DTM collected after the third run. The area shown covers 60°S to 90°S. Grid spacing is 5° in latitude, 10° in longitude. The DTM exhibits errors in the concentric ringlike features seen in some areas where models do not overlap adequately.

4 MARS

Stereoimagery from the Viking Orbiter missions has been used extensively for topographic mapping of Mars in the past, at scales ranging from regional (Howington-Kraus et al., 1995; USGS, 1996) to global (USGS, 1991). In light of the tremendous revolution currently underway in our knowledge of martian topography, driven by results from the Mars Orbiter Laser Altimeter (MOLA: Smith et al., 1998; 1999), it may seem paradoxical that we have recently initiated a project to collect regional-scale digital topographic models from Viking imagery. In fact, as has also been recognized

by others (e.g., Schenk and Moore, 1999; Cook et al., 2000a) the Viking stereo and MOLA datasets are highly complimentary. The greatest assets of the MOLA dataset are its globally distributed coverage and exceptionally high vertical precision: the range precision of a single measurement is less than 1 m, and orbit adjustment based on the analysis of crossing altimetry tracks leads to an absolute topographic accuracy on the order of 10 m (Smith et al., 1999). Within individual profiles the elevation measurements are spaced on the order of 300 m apart, but for many purposes the effective resolution of MOLA topography is limited by the spacing between adjacent profiles, which is expected to approach 1.5–2 km at the equator by the end of mission (with closer spacing at high latitudes). Photogrammetric analysis of the Viking images by themselves cannot approach the absolute accuracy of MOLA but can produce DTMs with useful vertical estimated precision (EP) and better horizontal resolution. Moreover, by incorporating MOLA-derived vertical control, the photogrammetric DTMs can achieve an absolute accuracy that is practically limited by their precision.

The greatest practical difficulty in stereomapping with Viking Orbiter data is data selection. Viking Orbiters 1 and 2 collectively returned more than 46,000 images of Mars between 1976 and 1980 (Snyder, 1977; 1979). Numerous observation sequences with different objectives resulted in an extremely complex and heterogeneous image set. Digital databases of the VO images include flat tables of metadata on CD-ROM with the images (Guinness et al., 1990) and the PDS Mars Geoscience Navigator (<http://wundow.wustl.edu/marsnav/>), which allows graphical and forms-based searching for particular images but does not provide an easy way to compare images and identify stereo pairs. A hardcopy catalog of potential stereopairs exists (Blasius et al., 1982) but is difficult to use and does not show stereo coverage in relation to surface features. Unpublished hemispheric maps of the highest resolution image coverage provide another fragment of useful information. None of these resources incorporate updated information about image locations that is generated as a byproduct of mapping. To better support our topographic mapping activities we have therefore created a simple yet flexible database of the VO images by extracting a subset of geometric metadata from the most up-to-date records at the USGS, Flagstaff, and writing customized software to analyze and display selected aspects of these data (Kirk et al., 1999a). The most important operations are the following.

- Matching the database files to a list of image identifiers (PICNOs) to extract images on (or *not* on) the list.
- Extracting data for images that intersect a given latitude-longitude zone.
- Creating a raster map of Mars showing the value of one of the geometric parameters (e.g., incidence angle) or a quantity computed from those parameters for the “best” image at each point, where “best” is defined by the extreme value of the same or another parameter (e.g., smallest resolution).
- Examining all possible pairs of images and creating a database of those that form acceptable stereo pairs.
- Creating a raster map showing the quality of stereo imagery.

Standard ISIS tools can be used to manipulate the raster maps further, for example, to color-code parameter data and superimpose them on a base image, or to calculate histograms of the parameters from maps in equal-area projection. The determination of suitable stereo coverage and quantification of its quality closely follows that of Cook et al. (1996) for Clementine, although at present we take an inclusive approach to allowing somewhat larger illumination differences and a variety of color-filter combinations. These factors (along with atmospheric clarity and surface changes such as frost deposition, which are not captured in the database) can be evaluated during mapping and unsuitable image pairs eliminated if necessary. Figure 3 shows histograms of the cumulative fraction of Mars covered by Viking images of given resolution, and by stereopairs of given EP. Readers can interactively examine the spatial distribution of coverage

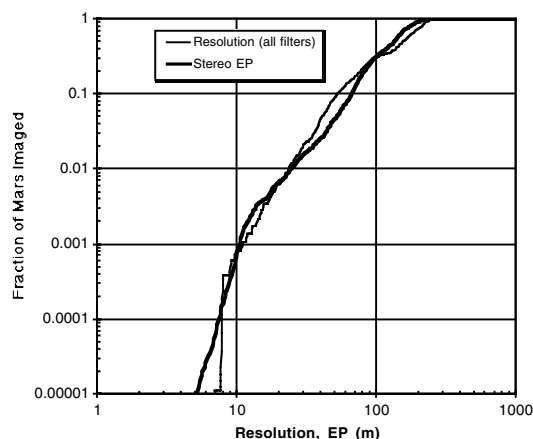


Figure 3. Fraction of Mars covered by Viking Orbiter images with given or better resolution and stereo precision EP.

by accessing the Planetary Interactive GIS Web-Analyzable Database (PIGWAD: Hare and Tanaka, 1999) at <http://webgis.wr.usgs.gov/>. It is clear from Figure 3 that the vertical precision of Viking stereo approaches 10 m for a small but significant portion of Mars (>100,000 km²) and is less than 100 m for roughly a third of the planet; depending on local relief, even vertical precisions of several hundred meters can be geologically useful. The horizontal resolution of the DTMs that can be realized from these stereopairs is not shown in Figure 3 but is roughly an order of magnitude larger than the EP (for stereopairs with a parallax-height ratio on the order of unity, as is typical). Thus, there is widespread Viking stereo coverage capable of yielding DTMs with horizontal resolution ≤ 1 km and therefore of improving on the resolution of the MOLA dataset.

We have recently begun topographic mapping of part of the Margaritifer Sinus region (latitude 17.5°S to 7.5°S, longitude 20°W to 25°W) and of Tithonium Chasma (latitude 7.5°S to 2.5°S, longitude 80°W to 85°W). These areas were selected in

consultation with the NASA Planetary Cartography/Geologic Mapping Working Group and its Geologic Mapping Subcommittee (GEMS). Topographic mapping of Margaritifer Sinus supports geological mapping and studies of the small valley networks in the area. The Tithonium map represents a start on collection of a detailed DTM for the entire Valles Marineris canyon system; in addition, since this area was previously mapped with hardcopy photogrammetric techniques (USGS, 1996), we will use the project to document the improvements in both efficiency of map compilation and precision and detail of the resulting product obtained by softcopy means. The Viking images used in the Margaritifer maps have resolutions of 170–340 m/pixel and yield vertical precisions of 80–150 m, while the images in Tithonium Chasma have resolutions of 60–150 m and EP of 70–130 m, compared to EP of 180–700 m for the stereomodels used to compile the previous map (USGS, 1996). As indicated above, vertical control for the maps will be based on MOLA data; we will interpolate elevations between individual altimetry profiles, although if the MOLA team releases an interpolated dataset with a grid spacing finer than the current 1° (Smith et al., 1999) this may be usable in less rugged areas. Planimetric control for the maps of these areas will be achieved by tying the stereoimages to the ~ 250 -m/pixel images in our newly revised global mosaic (Kirk et al., 2000), in which systematic errors in the previous version of the mosaic (Kirk et al., 1999b) have been eliminated and random errors have been reduced to ≤ 1 km globally. Orientation parameters for the global-mosaic images will be held fixed at the values determined by computation of the RAND-USGS control network of Mars (Davies et al., 1999a; 1999b). This network uses MOLA data to constrain the elevation of the majority of control points, and should therefore be consistent with the use of MOLA for vertical control in the regions of interest. However, the MOLA data currently incorporate the previously accepted value of the rotational parameter W_0 (Davies et al., 1996) which was based on an identification of the Viking 1 landing site (Morris and Jones, 1980) now known to be incorrect (Zeitler and Oberst., 1999; Parker and Kirk, 1999). The RAND-USGS network is tied to the well-identified Mars Pathfinder landing site and is consistent with the new site identification for Viking 1 (Parker and Kirk, 1999), so that the MOLA data must be shifted by about 0.15° in longitude to bring the two datasets into registration. Despite the widespread use of the MOLA data with their current longitude definition, we believe it is important to adopt planimetric control tied to the RAND-USGS network, which has been adjusted to conform to the IAU definition that the prime meridian of Mars passes through the crater Airy-0 (deVaucouleurs et al., 1973) as the latter is expected to remain the standard of longitude for the foreseeable future.

5 VENUS

Because of the enormous volume of data (~ 30 Gbytes) in the Magellan stereo images of Venus, digital mapping with automatic matching techniques is essential if more than a tiny fraction of the dataset is to be exploited. During and after the Magellan mission, we had the opportunity to experiment with two digital photogrammetric systems developed for Venus mapping: the Magellan Stereo Toolkit (MST) developed by VEXCEL (Curlander and Maurice, 1993) and the SAIC Digital SAR Workstation-Venus (DSW-V) (Wu and Howington-Kraus 1994). We found that neither package performed adequately for systematic mapping. The SAIC DSW-V was incapable of automatic matching of Magellan images. VEXCEL's MST had a usable matching algorithm, but lacked a rigorous sensor model, and the version we were able to use also lacked stereo display and interactive terrain editing capability. It was therefore considered highly desirable to develop a Magellan mapping capability within our SOCET SET-based DSW system. The main requisite of this capability is a sensor model that reflects the unusual properties of the Magellan SAR instrument (most notably, burst-mode operation in an elliptical orbit over a large range of altitudes). LH Systems provides a "generic" SAR model, but it requires large amounts of ground control and is not flexible enough for use with Magellan data. We therefore undertook the development of a Magellan-specific sensor model for SOCET SET by programming in the SOCET SET Developer's Toolkit.

5.1 Magellan Mission and Data

The Magellan spacecraft went into Venus orbit in 1990 and by 1992 had made three complete 8-month cycles of polar orbits, each cycle covering the full range of longitudes. During this time the spacecraft obtained synthetic aperture radar (SAR) images of $>96\%$ of the planet at a pixel scale of 75 m (Saunders et al., 1992). Images taken with a decreased look angle from vertical, primarily during Cycle 3, provide stereo coverage of 17% of the planet (~ 80 million km^2) when combined with images with same-side illumination from earlier in the mission. The stereo geometry of these images is extremely favorable, allowing elevation measurements with an estimated vertical precision (EP) of ~ 10 m (Leberl et al., 1992). Magellan also obtained radar altimetry data at a horizontal resolution varying from 8×10 km at periapsis to 30×20 km at the north pole, or 1–2 orders of magnitude coarser than can be achieved by stereomapping. The altimetry data is nevertheless useful for vertical control in mapping, as the average radius error after a reanalysis of spacecraft tracking and orbit data is on the order of 16 m (Rappaport et al., 1999). Magellan image and altimetry data were produced in a variety of formats with an "alphabet soup" of names (Pettengill et al., 1991); unfortunately, a discussion of our approach to Venus mapping necessitates a knowledge of some of this terminology. The F-BIDR (Full-resolution Basic Image Data Record) is the basic Magellan image product, containing a strip of SAR data from a single orbit, 30 km wide by up to 15,000 km long. Mosaics of imagery from multiple orbits were made both at full

resolution and with pixels averaged in blocks of 3x3, 9x9, and 27x27. These products were referred to as F-MIDRs, C1-, C2-, and C3-MIDRs (Full-resolution and Compressed Mosaicked Image Data Records) respectively. The pixel-averaged C-MIDRs were produced for all areas of Venus but only a subset of possible F-MIDRs were made. After the mission, the USGS produced a planetwide set of full-resolution mosaics (FMAPs) with a different data format and tiling scheme. The single strips (F-BIDRs), mission mosaics (MIDRs) and USGS mosaics (FMAPs) are thus the three types of images available for mapping. Altimetry data were archived orbit-by-orbit in vector format (ARCDRs) but for control we have relied on the global altimetric dataset gridded at 4.64 km/pixel, known as the GTDR.

5.2 Sensor Model

A sensor model is a function that specifies the transformation between image space (lines, samples) and object or ground coordinates (latitude, longitude, elevation). In addition to the image-to-ground function and its inverse (one of the two can be implemented numerically, given the other) a complete sensor model for SOCET SET contains 9 other functions, most of which carry out data input/output and bookkeeping functions.

Development of our Magellan SAR sensor model drew heavily on our experience creating a similar model for the SAIC DSW-V (Wu and Howington-Kraus, 1994) The model includes all the physics of the Magellan imaging process, and accounts for partial orthorectification of the images during correlation: distortions attributable to topography were removed (but only those accounted for in the very low resolution pre-Magellan topographic model) and must be put back in for the images to be matched correctly. Specifically, for a given ground point, the sensor model first determines which orbit strip (BIDR) the ground point is contained in, and then which radar burst from that BIDR. Once the radar burst is identified, the burst resampling coefficients and spacecraft position and velocity at the time of observation are known. Second, the range and doppler coordinates that the ground point was observed at are then calculated based on the spacecraft position and velocity at the time of observation. (This is the physical process of image formation that we must model.) In addition, the range coordinate is corrected for atmospheric refraction. Finally, the resampling coefficients associated with the burst are applied to the range and doppler coordinates to determine the image coordinates ("C1-C2" or line and sample) at which this range and doppler point were put into the image.

We have designed our system so that the sensor model will work with any combination of unmosaicked (F-BIDR), mission-mosaicked (F- and C-MIDR), and USGS-mosaicked (FMAP) images. We defined a SOCET SET Magellan dataset as an image containing data from an arbitrary number of original BIDRs, and a database relating the radar parameters to the footprint of each orbit and burst on Venus. The SOCET SET dataset will always be in Sinusoidal map projection, but its scale, center longitude, and extent can be arbitrary, depending on the product from which it was created. A library of BIDR header information from the BIDR tapes in Flagstaff is being built and is a one-time-effort. The library will provide the burst information whether one is processing data derived from BIDRs or from mosaics.

5.3 Spacecraft Ephemerides

Spacecraft position and velocity stored in the BIDR labels are known to contain significant errors. Orbit solutions were computed during the mission based on tracking data for blocks of eight orbits. North-south and east-west offsets of approximately 5 km between adjacent images from different blocks resulted. In the stereomapping process, the mismatches lead to "cliffs" between the blocks.

Our sensor model easily allows for the incorporation of improved spacecraft ephemeris while using existing image data and resampling coefficients. Using improved spacecraft ephemeris more accurately models the range and doppler that a ground point would actually have been observed at. While the resampling coefficients stored in the BIDR labels used to find the image pixel are "wrong" in the sense that they were based on bad ephemeris data, they are "right" in that they describe where range and doppler points were really put into the images during correlation.

Two sources of improved spacecraft ephemerides exist. The first consists of a block of ~50 Cycle 1 and Cycle 3 orbits over Maxwell Montes for which Paul Chodas at JPL has improved the orbit determinations and largely eliminated the "cliffs" by an adjustment process that includes tiepoints measured between overlapping images and recorrelation of the SAR images with the new orbit data (Chodas et al., 1993). Applied locally, this technique removes mismatches between images but may retain systematic errors affecting the whole block of images; tiepointing and recorrelating the global set of images to address this problem would require substantial effort. Second, reprocessing of the orbital tracking and navigation by Rappaport et al. (1999) in light of an improved gravity model (Konopliv et al., 1996), but without using constraints from image tiepointing, has also resulted in significant improvements to the entire set of Magellan orbits. These new orbit solutions are based on the detailed gravity observations from the end of the mission. Errors in the ephemerides are decreased 1–2 orders of magnitude in all 3 axes by use of the new gravity model. The remaining radial errors are typically ≤ 1 m and are negligible, but along-track and cross-track errors are typically a few

hundred meters and for some orbits exceed 1 km. Errors of this magnitude can have a significant impact on stereomapping: across-track errors will lead to errors in the estimated ground elevations (as well as east-west positioning errors), while along-track errors can introduce spurious y-parallax and prevent stereo fusion. In anticipation that available ephemerides may not suffice for mapping, we have designed our Magellan sensor model so that SOCET SET's bundle-block adjustment module can be used to adjust each BIDR by along-track, cross-track and radial translations varying linearly with time. This type of low-order correction should be adequate to bring small regions of imagery into agreement with the altimetry data. One of our goals is to evaluate the absolute and relative precision of the tiepointed (Chodas et al., 1993) and gravity-derived (Rappaport et al., 1999) ephemerides as they affect mapping, and, if necessary, develop the procedures for performing local orbit adjustments with SOCET SET.

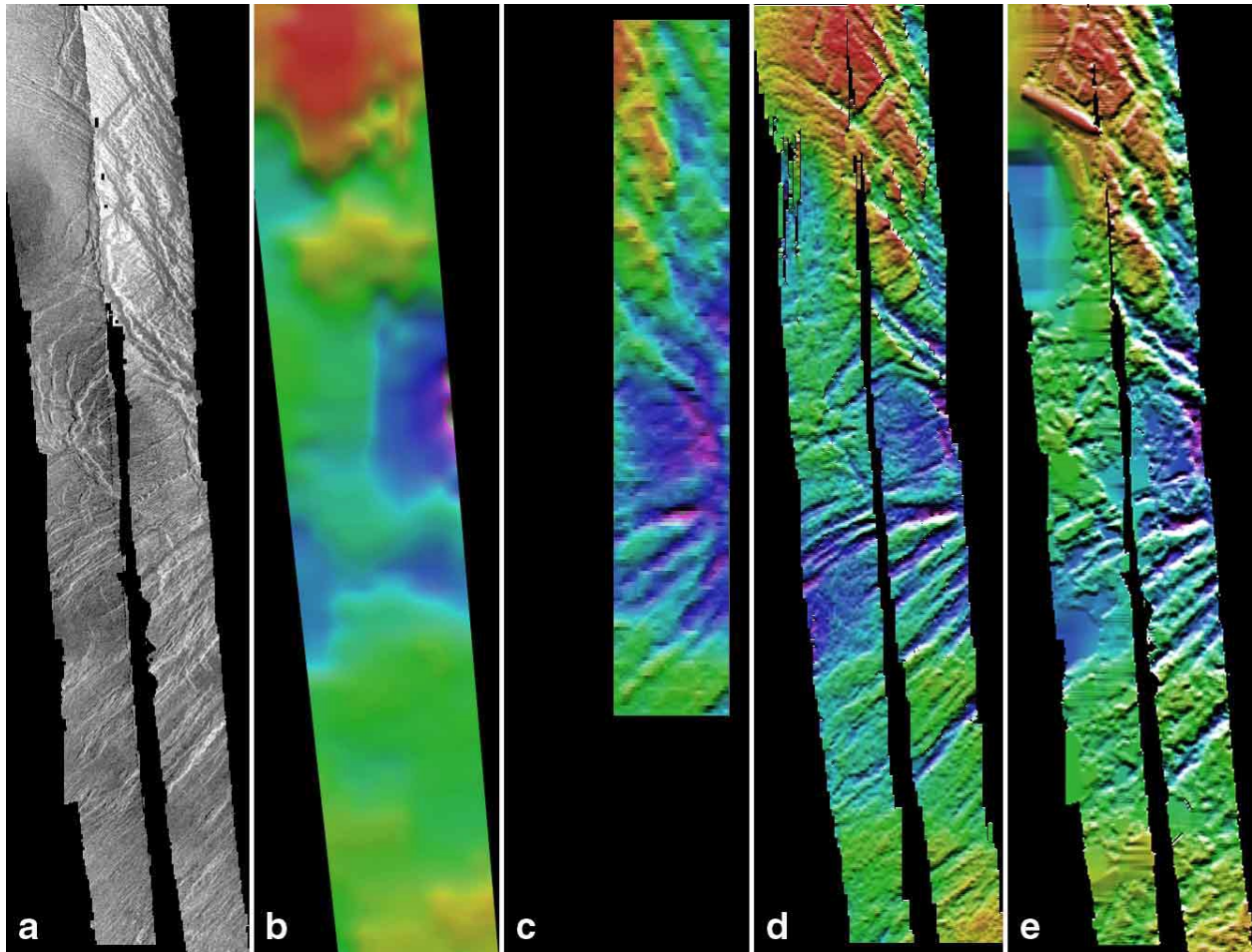


Figure 4. Comparison of results of mapping Magellan stereo test area (3°S–0°, 73°E–73.5°E). (a) orthomosaic of Cycle 3 images 2674 and 2675. Remaining images are color shaded relief portrayals of DTM data (color range is the same for all DTMs and represents 2.3 km of elevation). (b) portion of global gridded altimetry (GTDR); (c) DTM obtained with VEXCEL MST software from mosaicked images; (d) DTM obtained with SAIC DSW-V software by manual extraction; (e) DTM obtained with SOCET SET automatic terrain extraction, after interactive editing.

5.4 Test Results

Testing of our Magellan sensor model includes not only validation of the sensor model, but specific comparison of the quality of results obtained with the different orbit solutions. To date three test areas have been visited.

Orbits 877-878 and 2674-2675 (Stereo Test): Orbits 877-878 and 2674-2675 cover the stereo test area acquired during Cycle 2 of the Magellan mission and were previously used to test the SAIC DSW-V and the VEXCEL MST systems. (VEXCEL MST does not process individual BIDRs, so appropriate subareas of mosaics were used.) DTMs obtained with the three systems are shown as color shaded relief images in Figure 4, along with a DTM derived from the gridded altimetry and an

Photogrammetric System	Year	DTM Resolution	Extraction Time
LH Systems DSW	1999	375 m	2 min
VEXCEL MST	1996	600 m	25 min
SAIC DSW-V	1993	587 m	40 hrs

orthomosaic of the Cycle-2 images. The latitude and longitude range mapped was approximately 3°S to 0°, 73°E to 73.5°E. We find that the SO CET SET matcher combines high DTM resolution with high speed (Table 5). Some manual editing was necessary in bland areas of the images where automatic stereomatching did not produce useful results, so the actual time required for mapping was on the order of an hour per stereopair. The overall mapping efficiency (in elevation measurements collected per workday) still greatly exceeds that of the other two systems tested.

FMAP 06S066 (Joliot-Curie): The Joliot Curie FMAP covers latitudes 12°S to 0° and longitudes 60°E to 72°E, and contains 64 orbits in the Cycle 1 mosaic, and 53 orbits in the Cycle 3 mosaic. This dataset was previously chosen for evaluation of the VEXCEL MST software because of the extensive stereo coverage and diverse, scientifically interesting terrain covered, which includes tesserae of western Ovda Regio, some smooth plains, the 100-km crater Joliot-Curie, and a circular volcanotectonic structure (corona) of similar size. This region provided our first test of mapping with mosaicked images in SO CET SET. The sensor model performed well with regards to tracking which orbit a pixel came from. Residual along- and across-track errors in the ephemerides from Rappaport et al. (1999) were sufficient to prevent automatic terrain extraction from working. We are working on procedures needed to adjust the individual orbits based on tiepointing of the BIDs in this area and then apply the derived corrections to the mosaics. Mapping from the mosaics is desirable because it involves a much smaller set of image files and hence much less work manually defining the areas to be mapped in each stereopair. In the interim, we manually extracted a DTM of part of the Joliot-Curie quadrangle at a ground sample distance of 3375 m (45 pixels), which is much coarser than ultimately desired but still almost an order of magnitude better than the resolution of the Magellan altimeter. We compared elevation values of the resulting DTM with the corresponding altimetry data. In flat areas, the two are in agreement, but the stereo DTM is higher in areas of tessera, which consist of troughs and valleys with a local elevation range of ~500 m. To a good approximation, the altimetry data follow the valley bottoms of the stereo DTM. This was initially unexpected because it is common in processing radar altimetry data to report the position of the first detected echo, which in tessera terrain would correspond to the ridge tops. However, the Magellan gridded altimetry dataset is derived from the strongest echo detected for each foot print (the ungridded ARCDR dataproducts record both the first and strongest echos) and in tessera terrain this commonly corresponds to the valley bottoms (P. G. Ford, written communication, 2000). The discrepancy between the altimetric elevations and the valley floors in our DTM is consistent with the height-error introduced by the known across-track uncertainty of the ephemerides used (Rappaport et al., 1999) and could be removed by a local adjustment calculation.

Orbits 512-536 and 4075-4106 (Maxwell): Chodas, Rappaport and original mission ephemerides are available for orbits 512-536 and 4075-4106 which cover Maxwell Montes. We recently reported (Howington-Kraus et al., 2000) finding a large north-south offset between the Cycle-1 and Cycle-3 images in this area that prevented stereo fusion and mapping. We have been able to trace this relative offset to a programming error in our handling of map-grid coordinates when transferring data from ISIS to SO CET SET. However, in the course of investigating this error we found another, more subtle problem that seems to affect the computed latitude coordinates of all images in all cycles. Our software does not compute the same latitude for a pixel in the BIDR as is recorded in the BIDR labels, even when we use elevation coordinates and spacecraft ephemeris taken from the BIDR itself. In contrast, longitudes calculated from our software agree with those in the BIDRs. We are still investigating the causes of the discrepancy, which may reflect a bug in our software, inconsistencies in the BIDRs (we have demonstrated that some of the other data in the BIDRs are mutually inconsistent), or a combination. The magnitude of the north-south error is significant, approaching a kilometer at high latitudes. Since it affects both images of a given stereopair equally, however, it does not prevent us from testing the success of stereomatching with the various ephemeris solutions. Our initial results indicate that the Chodas ephemerides produce better agreement between overlapping images but contain significant absolute errors compared to the Rappaport ephemerides. The latter, though more accurate, yield image-to-image mismatches of a few pixels (i.e., 100–200 m, consistent with the estimated errors). A local adjustment based on tiepointing is therefore likely to be needed if the full accuracy of these ephemerides are to be exploited for mapping.

6 BEYOND: ASTEROID 433 EROS

On 14 February 2000, the Shoemaker NEAR spacecraft entered orbit around the 13x31 km asteroid 433 Eros, becoming the first artificial satellite of a minor body and beginning a year-long mission of morphologic and compositional mapping (Cheng et al., 1997). One of us (Kirk) was selected as a Participating Scientist on the NEAR Multispectral Imager (MSI) team (Veverka et al., 1997), with the task of producing high-resolution topographic models of Eros by photogrammetry and photoclinometry and interpreting the results in terms of small-scale surface features and processes. This is only one of several topographic investigations within the mission. The NEAR laser rangefinder (Zuber et al., 1997) will produce very accurate, high-resolution topographic profiles, but, as with MOLA, the interprofile spacing will limit the resolution of the global shape model that can be interpolated from these data. A global shape model has also been constructed from MSI data by a combination of manual and automatic stereo and limb-fitting techniques (Thomas et al., 2000) and will be updated as improved image coverage become available throughout the orbital

mission. This model, which consists a polyhedron with ~8000 facets or “plates,” will form the basis for coregistering a variety of datasets such as image mosaics and spectral and other compositional data, but does not have the resolution necessary to delineate small features such as impact craters, ridges, grooves, and blocks, all of which have been seen in early MIS images. Stereomapping will allow us to produce local DTMs of the surface of Eros at a lateral resolution of a few image pixels, while photoclinometry may later be used to refine these DTMs to single-pixel resolution (Giese et al., 1996). As this is written, NEAR is in a 200-km orbit, yielding 20 m/pixel images, but the altitude of the orbit will be successively reduced to 100 and eventually 50 km, so that a substantial fraction of the asteroid will be imaged at 5 m/pixel; thanks to the rotation of the asteroid and orbital motion of NEAR, these image sets will contain repeat coverage with excellent stereo viewing geometry (Veverka et al., 1997). First-order scientific questions to be addressed are, how do the sizes of features such as grooves, ridges and blocks compare with those seen on other small bodies? It appears that impact craters on asteroids Gaspra and Ida are anomalously shallow (Carr et al., 1994; Sullivan et al., 1996) and a variety of explanations have been advanced; is this true of Eros as well? Perhaps more exciting than the high resolution offered by the MSI images is the opportunity to obtain global coverage with consistent resolution and illumination slowly changing over Eros’s seasons. Flyby investigations of asteroids such as Gaspra, Ida, and Mathilde in the past have left many questions about whether the varying appearance of parts of their surfaces represent geologic differences or only the nature of illumination. Detailed topographic mapping of Eros over the course of the NEAR mission will allow us to distinguish real variations from observation effects and perhaps begin to answer questions such as how the distribution of surface materials (regolith) on Eros are affected by the enormous variation in gravity between the center and ends of the body, and how such differences relate to compositional maps of the surface.

As always, the MSI data present several mission-specific features. For example, the 244x537-pixel CCD detector uses nonsquare pixels, so that the images must have their aspect ratio rectified before photogrammetric processing (Veverka et al., 1997). The biggest challenges posed by the dataset, however, are those of selecting images to work with and setting up appropriate coordinates for data collection, both of which are influenced by the complex motion of NEAR in orbit around a highly irregular object that is also rotating with a period of 5.27 hours. The MSI is being used to obtain systematic sets of images spaced throughout each rotation of Eros. In the current orbit, successive sequences of this kind taken together yield good stereo convergence; each sequence shows most of the visible side of Eros, so recognizing the areas covered is not a problem. As the orbit is lowered, however, the problem of identifying images of the same small patch of surface will become more complex. Once stereopairs are selected, collection of DTM data requires care in establishing appropriate coordinates. SOCET SET is optimized for mapping the Earth with vertical imagery, and its DTM datastructure cannot represent the complete surface of an irregular body like Eros. Fortunately, we have already encountered this problem with the Mars Pathfinder panoramic stereo images (Kirk et al., 1999c) and solved it in practice by establishing a “local” coordinate system for each stereopair with coordinate axes along and perpendicular to the stereobase. The situation for NEAR is essentially that of Pathfinder turned “inside out”: rather than a rotating camera imaging 360° of surrounding terrain, we are imaging a rotating body from a camera on a path encircling it. Control for the stereomodel is obtained by transforming laser rangefinder or MSI-derived global shape data from global coordinates into the local system. Once a DTM of a patch of surface is collected from a single stereopair in “local” coordinates, we use ISIS software to transform each datapoint individually into the global coordinate system (Eros body-centered or universal space rectangular) where they can be merged with other such data. For applications such as measuring the depths of impact craters, however, the local-coordinate DTMs may be used directly.

7 CONCLUSIONS

The case studies presented here suggest three general conclusions. First, the utility of quantitative topographic information to the study of planetary surfaces can hardly be overemphasized. Topography bears directly on geologic history and on identifying and understanding the importance of surface processes such as impact modification, volcanism, and eolian, fluvial and glacial erosion. Second, although we are entering an era in which planetary missions are increasingly making use of laser altimetry, this does not indicate the end of stereophotogrammetric mapping of the planets. Rather, there is a strong synergy between the two types of dataset, and stereomapping will continue to be useful as a source of topographic data of very high horizontal resolution for areas of interest. The challenge will be to develop techniques that exploit the high absolute accuracy of the altimetric data to constrain photogrammetric solutions and improve their reliability. (Similar comments apply *a fortiori* to photoclinometry, which produces topographic models that are even more detailed than those from photogrammetry but have even worse absolute accuracy and are even more expensive to produce.) Finally, planetary photogrammetry continues to offer a host of unique challenges: nearly every dataset has crucial differences in format, coverage, and quality that make it necessary to continually innovate new approaches to data selection, generation of control, and extraction of topographic data. We have found the combination of in-house software tailored to processing of planetary image data with commercial softcopy photogrammetric software to be a powerful one for addressing these challenges. The commercial software provides a host of tools for steps such as bundle-block adjustment, automatic terrain extraction, and interactive editing of

dataproducts with stereo display that make topomapping possible and relatively efficient, but would be extremely tedious to develop. Access to an in-house software system dedicated to planetary image processing, on the other hand, provides both a suite of existing tools for mission- and instrument-specific processing and an environment in which we can rapidly develop additional such tools as needed. Programming on the interface between the two systems is especially important to exploiting the strengths of both.

ACKNOWLEDGMENTS

Project funding and support is provided by NASA's Research Opportunities in Space Science, Planetary Geology and Geophysics Program and by the NEAR Participating Scientist Program. The authors wish to acknowledge programming support from Trent Hare, and the work of Bonnie Redding and Donna Galuszka in collecting and editing DTMs and match points.

REFERENCES

- Batson, R. M., and E. M. Eliason, 1991. Digital Maps of Mars. *Photogramm. Eng. & Remote Sens.*, 61, pp. 1499–1507.
- Blasius, K. R., A. V. Vetrone, and M. D. Martin, 1982. Viking Orbiter Stereo Image Catalog, NASA CR 3501, 404 pp.
- Carr, M. H., R. L. Kirk, A. S. McEwen, J. Veverka, P. C. Thomas, J. W. Head, and S. Murchie, 1994. The geology of Gaspria. *Icarus*, 107, pp. 61-71.
- Cheng, A. F., et al., 1997. Near-Earth Asteroid Rendezvous: Mission overview. *J. Geophys. Res.*, 102(E10), pp. 23,695–23,708.
- Chodas, P. et al., 1993. Title. AAS/AAJA Astrodynamics Specialist Conference, (accessed at <http://techreports.jpl.nasa.gov>).
- Cook, A. C., J. Oberst, T. Roatsch, R. Jaumann, and C. Acton, 1996. Clementine imagery: selenographic coverage for cartographic and scientific use. *Planet. Space Sci.*, 44(10), pp. 1135-1148.
- Cook, A. C., and M. S. Robinson, 1999. Digital elevation models of the lunar surface. In: *Workshop on New Views of the Moon II: Understanding the Moon Through the Integration of Diverse Datasets*. LPI Contribution No. 980, Lunar and Planetary Institute, Houston.
- Cook, A. C., D. Mege, and R. A. Craddock, 2000a. Stereo derived digital elevation models of Mars fitted to to MOLA profiles. *Lunar Planet. Sci.*, XXXI, Abstract 2008, Lunar and Planetary Institute, Houston (CD-ROM).
- Cook, A. C., P. D. Spudis, M. S. Robinson, T. R. Watters, and D. B. J. Bussey, 2000b. Lunar polar topography derived from Clementine stereo imagery, *Journal of Geophysical Research*, in publication.
- Curlander, J., and Maurice, K., 1993. Magellan Stereo Toolkit User Manual (unpublished), VEXCEL Corporation, Boulder, Colorado.
- Davies, M. E., et al., 1996. Report of the IAU/IAG/COSPAR Working Group on Cartographic Coordinates and Rotational Elements of the Planets and Satellites: 1994. *Celestial Mechanics and Dynamical Astronomy*, 63, pp. 377–397.
- Davies, M., T. Colvin, R. Kirk, E. Lee, and R. Sucharski, 1999a. Status of the RAND-USGS control network of Mars. In: *The Fifth International Conference on Mars*, LPI Contribution No. 972, Lunar and Planetary Institute, Houston (CD-ROM).
- Davies, M. E., T. Colvin, R. Kirk, E. Lee, R. Sucharski, and T. Duxbury, 1999b. The RAND-USGS control network of Mars and the martian prime meridian. *Eos Trans. AGU (suppl.)*, 80, p. F615.
- DeVaucouleurs, G., M. E. Davies, and F. M. Sturms, Jr., 1973. Mariner 9 areographic coordinate system. *J. Geophys. Res.*, 70(20), pp. 4395–4404.
- Duxbury, T. W., et al., 1999. MOLA: The future of Mars global cartography. In: *The Fifth International Conference on Mars*, LPI Contribution No. 972, Lunar and Planetary Institute, Houston (CD-ROM).
- Eliason, E.M., 1997. Production of digital image models using the ISIS system. *Lunar Planet. Sci.*, XXVIII pp. 331-332, Lunar and Planetary Institute, Houston.
- Eliason, E.M., et al., 1999. Digital processing for a global multispectral map of the Moon from the Clementine UVVIS imaging instrument. *Lunar Planet. Sci.*, XXX Abstract 1933, Lunar and Planetary Institute, Houston (CD-ROM).
- Feldman, W. C., S. Maurice, A. B. binder, B. L. Barraclough, R. C. Elphic, and D. J. Lawrence, 1998. Fluxes of fast and epithermal neutrons from Lunar Prospector: Evidence for water ice at the lunar poles, *Science*, 281, pp. 1496–1500.

- Rappaport, N. J., A. S. Konopliv, A. B. Kucinskis, and P. G. Ford, 1999. An improved 360 degree and order model of Venus topography. *Icarus*, 139, pp. 19–31.
- Rosiek, M., R. Kirk, and A. Howington-Kraus, 1999a. Lunar topographic maps derived from Clementine imagery. *Lunar Planet. Sci.*, XXX Abstract 1853, Lunar and Planetary Institute, Houston (CD-ROM).
- Rosiek, M., R. Kirk, R., and A. Howington-Kraus, 1999b. Lunar south pole topography derived from Clementine imagery. In: *Workshop on New Views of the Moon II: Understanding the Moon Through the Integration of Diverse Datasets*. LPI Contribution No. 980, Lunar and Planetary Institute, Houston.
- Rosiek, M., R. Kirk, and A. Howington-Kraus, 2000. Digital elevation models derived from small format lunar images. *Tech. Papers of the Annual Meeting of the ASPRS*, in publication.
- Saunders, R. S., et al., 1992. Magellan mission summary. *J. Geophys. Res.*, 97(E8), pp. 13,067–13,090.
- Schenk, P. M., and J. M. Moore, 1999. Stereogrammetric mapping of Mars: Promise, progress, and problems. In: *The Fifth International Conference on Mars*, LPI Contribution No. 972, Lunar and Planetary Institute, Houston (CD-ROM).
- Simpson, R. A., and G. L. Tyler, 1999. Reanalysis of Clementine bistatic radar data from the lunar south pole. *J. Geophys. Res.*, 104, p. 3845–3862.
- Smith, D. E., M. T. Zuber, G. A. Neumann, and F. G. Lemoine, 1997. Topography of the Moon from the Clementine lidar. *J. Geophys. Res.*, 102(E1), pp. 1591–1611.
- Smith, D. E., et al., 1998. Topography of the northern hemisphere of Mars from the Mars Orbiter Laser Altimeter. *Science*, 279, pp. 1686–1692.
- Smith, D. E., et al., 1999. The global topography of Mars and implications for surface evolution. *Science*, 284, pp. 1495–1503.
- Snyder, C. W., 1977. The Missions of the Viking Orbiters. *J. Geophys. Res.*, 82, pp. 3971–3983.
- Snyder, C. W., 1979. The Extended Mission of Viking. *J. Geophys. Res.*, 84, pp. 7917–7933.
- Sullivan, R., et al., 1996. Geology of 243 Ida. *Icarus*, 120, pp. 119–139.
- Thomas, P. C., J. Joseph, B. Carcich, B. E. Clark, J. Veverka, J. K. Miller, W. Owen, and B. Williams, 2000. The shape of Eros from NEAR imaging data. *Icarus*, in publication.
- Torson, J., and K. Becker, 1997. ISIS: A software architecture for processing planetary images. *Lunar Planet. Sci.*, XXVIII, pp. 143–1444, Lunar and Planetary Institute, Houston.
- U.S. Geological Survey, compiler, 1991. *Mission to Mars: Digital Topographic Map*, PDS Volume USA_NASA_PDS_VO2007 (CD-ROM).
- U.S. Geological Survey, compiler, 1996. *Topographic map of the Tithonium Chasma region of Mars*. USGS Open File Report #96-714.
- Veverka, J., et al., 1997. An overview of the NEAR multispectral imager-near infrared spectrometer investigation. *J. Geophys. Res.*, 102(E10), pp. 23,709–23,727.
- Wählisch, M., H. Hoffmann, R. Wagner, U. Wolf, A. Hoffmeister, and R. Jaumann, 1999. High resolution mosaic and digital terrain model in the lunar south pole region derived from Clementine data. *Lunar Planet. Sci.*, XXX, Abstract 1636, Lunar and Planetary Institute, Houston (CD-ROM).
- Wu, S. S. C., 1975. *Topographic mapping of Mars*. U.S. Geological Survey Interagency Report: Astrogeology 63.
- Wu, S. S. C., and F. J. Doyle, 1990. *Topographic mapping*. In: *Planetary Mapping* (Ronald Greeley and R. M. Batson, eds.). Cambridge Univ. Press, Cambridge, pp. 169–207.
- Wu, S.C., and E. A. Howington-Kraus, 1994. Magellan radar data for Venus topographic mapping. *Lunar Planet. Sci.*, XXV, pp. 1519–1520, Lunar and Planetary Institute, Houston.
- Zeitler, W., and J. Oberst, 1999. The Mars Pathfinder landing site and the Viking control point network. *J. Geophys. Res.*, 104(E4), pp. 8935–8942.
- Zuber, M. T., D. E. Smith, F. G. Lemoine, and A. G. Neumann, 1994. The shape and internal structure of the Moon from the Clementine mission. *Science*, 266, pp. 1848–1851.
- Zuber, M. T., D. E. Smith, A. F. Cheng, and T. D. Cole, 1997. The NEAR laser ranging investigation. *J. Geophys. Res.*, 102(E10), pp. 23,761–23,773.